Determination of Cleavage Energy and Efficient Nanostructuring of Layered Materials by Atomic Force Microscopy

Bertold Rasche, Julius Brunner, Tim Schramm, Madhav Prasad Ghimire, Ulrike Nitzsche, Bernd Büchner, Romain Giraud, Manuel Richter, Joseph Dufouleur

Determination of Cleavage-Energy and Efficient Nanostructuring of Layered Materials by Atomic Force Microscopy

Bertold Rasche,*,† Julius Brunner,‡ Tim Schramm,‡ Madhav Prasad Ghimire,¶ Ulrike Nitzsche,‡ Bernd Büchner,‡ Romain Giraud,‡ Manuel Richter,‡ and Joseph Dufouleur*,‡

†*Department of Chemistry, University of Cologne, 50939 Cologne, Germany*

‡*Leibniz IFW Dresden, Helmholtzstr. 20, D-01069 Dresden, Germany*

¶*Central Department of Physics, Tribhuvan University, Kirtipur, 44613, Kathmandu, Nepal*

§*Dresden Center for Computational Materials Science (DCMS), TU Dresden, D-01062 Dresden, Germany*

E-mail: bertold.rasche@uni-koeln.de; j.dufouleur@ifw-dresden.de

Abstract

A method is presented to use atomic force microscopy to measure the cleavage energy of Van-der-Waals- and similar quasi two-dimensional materials. The cleavage energy of graphite is measured to be $0.36\,\mathrm{J/m^2}$, in good agreement with literature data. The same method yields a cleavage energy of $0.6\,\mathrm{J/m^2}$ for MoS_2 as a representative of the dichalcogenides. In case of the weak topological insulator $Bi_{14}Rh_3I_9$ no cleavage energy is obtained, although cleavage is successful with an adapted approach. The cleavage energies of these materials are evaluated by means of density-functional calculations and

literature data. This further validates the presented method and sets an upper limit of about $0.7\,\mathrm{J/m^2}$ to the cleavage energy that can be measured by the present setup. In addition, this method can be used as a tool for manipulating exfoliated flakes, prior or after contacting, which may open a new route for the fabrication of nanostructures.

Keywords

cleavage energy, Van-der-Waals Materials, two-dimensional materials, atomic force microscopy, nanostructuring

Quasi two-dimensional (2D) materials and the corresponding devices allow to study unexplored fields in fundamental condensed matter physics and are even expected to be at the heart of a forthcoming technical revolution. Started off with the fabrication of graphene,[1,2] a material with extraordinary mechanical and electronic properties, further examples include topological insulators,[3,4] few-layer transition-metal dichalcogenides,[5–11] nearly ideal 2D ferromagnets like $Cr_2Ge_2Te_6$,[12] and tilted bilayer graphene.[13,14] Ultra-thin device structures are frequently prepared by exfoliating such a layered (quasi-2D) material, as for the seminal case of graphene. The success of this procedure is based on very anisotropic chemical interactions implicating strongly bound, robust layers which are held together by weak, primarily Van-der-Waals, interactions. The physical phenomena studied, e.g., gate-induced superconductivity[7,8,15] or the quantum spin Hall effect in monolayers of WTe_2,[6,10] are related to the almost perfect 2D structure in the case of the monolayers, or, in case of few-layers, to the very anisotropic electronic interactions within the quasi-2D host structures.

Despite the strong interest in quasi-2D materials-based devices built out of few exfoliated layers, the measurement of the interlayer interactions has so far received little attention. While there is a manifold of theoretical investigations for various materials available,[16–28] experiments are scarce and have mainly been performed for graphite. Indeed, the latter has been characterized with several techniques.[16,29–36] However, most of these are specific for graphite since they exploit its unique properties such as the formation of nanotubes, the adsorption of polyaromatic hydrocarbons or the self-retraction phenomenon.[30–33,35] There-

fore, these methods cannot be used for other layered materials such as transition metal chalcogenides or layered topological insulators. Hence, measurements of the cleavage energy reported for any other material than graphite are laborious and involve a rather specific setup, such as a surface force balance.[36,37]

In contrast, atomic force microscopy (AFM) has proven to be a powerful and easy-to-use method in the handling and manipulation of quasi-2D materials[38–40] as e.g. for thinning down topological insulator nanoribbons of Bi_2Se_3.[41] Additionally, AFMs are widely available and can easily be accessed. In this work, we present a generic approach to determine the interlayer binding energy by measuring the lateral deflection force on an AFM tip during cleavage. To validate our approach, three characteristic quasi-2D materials are investigated: graphite, molybdenum disulfide (MoS_2), and the weak topological insulator $Bi_{14}Rh_3I_9$.[42–44] The experimental work is complemented by calculations based on density functional theory (DFT). As the experimental method involves only the use of an AFM, this approach can potentially be established as a standard and rather simple way for measuring interlayer binding energies. Finally, we demonstrate that this method can also be used to thin nanostructures of layered materials down to the few layers limit, establishing it as a suitable tool for nanostructuring.

A schematic illustration of the fabrication process of our samples is shown in Figure 1 a-c. In the following, we give a short summary of the process and refer to the supporting information (SI) for all further details. A single crystalline flake of the layered material is first mechanically exfoliated with PDMS-tape and transferred onto a silicon substrate (Si^{++}) covered by a thermally grown amorphous SiO_2 layer (Figure 1a). The size of the flakes after exfoliation is typically 200 µm in length and approximately 100 nm in height (Figure 1d). Second, the layered material is shaped into pillars. To this end, standard e-beam lithography is used to cover the crystal flake with a regular array of aluminum rectangles. The rectangles cover an area of 1 µm × 3 µm each (Figure 1b) and act as an etching mask during the subsequent argon etching process that leaves well-defined pillars

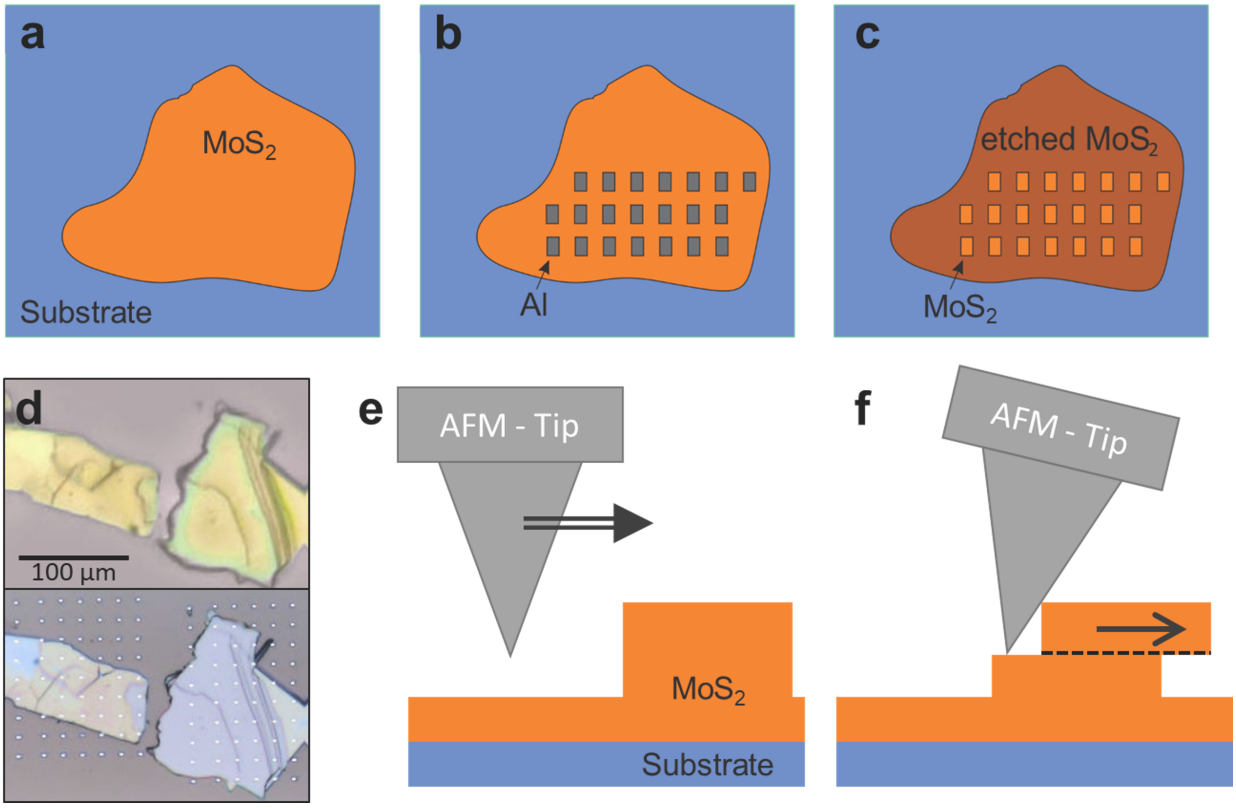

Figure 1: a) to c) Sketch of the fabrication of the samples with d) a light microscope picture of natural flakes and of flakes with the manufactured pillars on it (the squares beyond the natural flakes are pillars of the underlying SiO_2-substrate). e) and f) illustrate the process to determine the cleavage energy. Note that, the schematic figures apply to all materials, not only to the example MoS_2.

of the material under the aluminum mask (Figure 1c). The etching time is adjusted such that the flake material is not fully removed from the substrate to make sure that the base of the pillars lies on the material under investigation (Figures 1e and f). This is important to avoid the measurement of the (weak) adhesion energy between the material and the substrate instead of the cleavage energy. Finally, the aluminum is selectively removed with a highly concentrated aqueous NaOH solution. Squared pillars of about 50 nm height are hence fabricated at the surface of the crystals (Figure 1c and d) and the sample can be used to determine the cleavage energy of the material.

Determining the cleavage energy via our method involves integration of the tip forces during the cleavage process and thus makes it necessary to calibrate the cantilever. The

calibration allows one to convert the deflection of the tip measured in volts into a force and finally to calculate the cleavage energy. Following Hook's law, we assume proportionality between the normal deflection D and the corresponding normal force F_D, as well as the lateral deflection LD and the corresponding lateral force F_{LD}:

$$F_D = -\kappa \cdot D \tag{1}$$

$$F_{LD} = -\alpha \cdot LD \tag{2}$$

where κ and α are the normal and the lateral spring constant, respectively. The assumed linear behavior remains true as long as the bending of the cantilever and the twisting angle of the cantilever (tilting of the tip) remain small, which is usually true for AFM experiments.

The calibration of the normal spring constant κ of the cantilever (TAP300DLC, NanoAndMore; details see SI) is done with thermal noise calibration provided by the AFM software from Asylum Research (adapted Igor Pro 8). For the calibration of the lateral spring constant α, a method similar to the improved wedge calibration of Varenberg *et al.*[45] is used with a standard calibration grating from CalibratAR. The calibration procedure is described in detail in the SI, in particular in Figure SI 2. It has to be done once for each tip in order to determine the tip dependent values of κ and α.

Before the cleavage experiment, an AFM-image of the pillar is acquired in tapping mode (Figure 2a). Then, the cleavage of the pillar is performed using the "snap-litho"-mode of the Igor Pro software. As described above, a tip path is defined laterally to the cantilever axis at a fixed height (Z-sensor in Figure SI 3). The height should be adjusted at a level below the height of the pillar, such that the tip can cleave the crystal when travelling along the pre-defined path by hitting the pillar (Figure 1f). Using the lateral direction for the cleavage process allows to separate the cleavage force (tilting of the cantilever) from the force that acts perpendicular to the sample surface and bends the cantilever. As demonstrated in the SI (Figure SI 3) the cross-talk between the respective lateral and normal deflection is

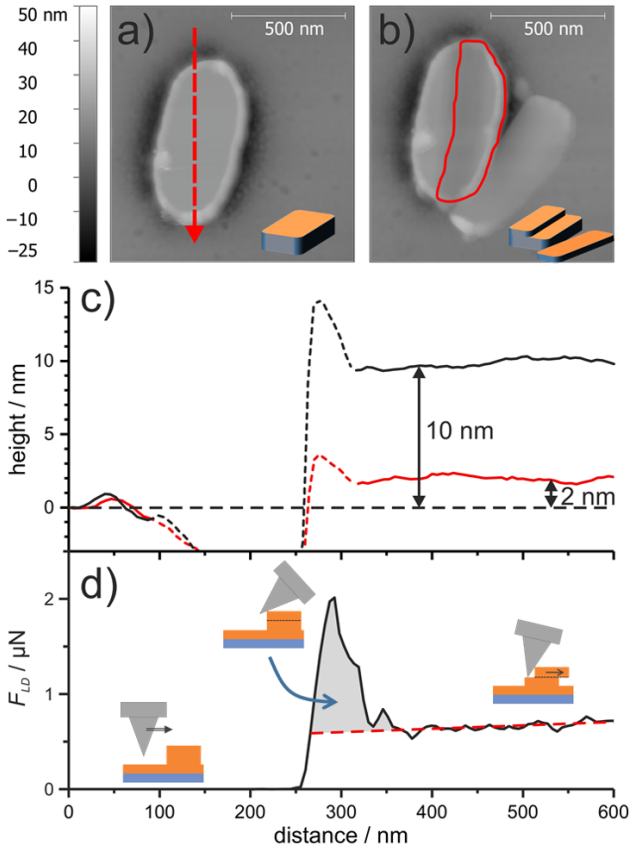

Figure 2: a) AFM image before and b) after an AFM cleavage process on a graphite pillar (dashed arrow represents the AFM cleavage path; red outline encircles the cleaved area). c) Height profile before (black) and after (red) the cleavage process. Dashed lines represent regions with artefacts of the AFM electronics due to a relatively high scan rate. d) Force curve (black) during the cleavage process, with a baseline (red dashed) and the integrated area for the energy determination (grey). For the latter curve, raw data of the Z-sensor, the lateral and normal deflection are shown in the SI Figure SI 3. Sketches illustrate the respective states of the cleavage process.

relatively small as long as the travelling path of the tip is oriented perfectly orthogonally to the orientation of the cantilever.

A typical height profile of a graphite pillar with the assigned height path and the corresponding AFM-picture are shown in Figure 2. The velocity of the tip should be low enough to acquire enough data points during the cleavage process but fast enough to ensure a sufficient success rate of the cleavage. A reasonable compromise was found to be a velocity of around 460 nm/s. The observation that a higher velocity leads to a higher success rate of the cleavage might be due to the higher momentum on impact of the tip into the material, which helps to overcome the activation energy of the cleavage process. This might be understood in similarity to the difference between static and dynamic friction, where the former would correspond to the initial activation of bond breaking, while the latter would correspond to the continuous breaking of further bonds without additional activation. After each attempt, an AFM-scan of the pillar is taken in tapping mode to check the success of the cleavage, meaning that part of the pillar has been removed from the initial pillar. The cleaved part of the pillar often folds upwards or lies in the vicinity of the pillar (Figure 2b; Figure SI 4 and 5). Simultaneously, part of or the whole pillar become lower (Figure 2c). The area of the cleaved part defines the cleavage surface A (see below) and is determined graphically (Figure 2b). The position-dependent lateral deflection LD is converted into a force (F_{LD}) as described above.

In Figure 2d a typical graph of the lateral force during a cleavage experiment is shown. A large peak can be identified when the tip hits the edge of the pillar. This peak is attributed to the force required to cleave the crystal. From integration of F_{LD} over the travelled path l using the deflection after the initial cleavage peak as baseline (Figure 2d), the cleavage energy can be calculated according to

$$E_{Cl} \cdot A = \int_{\text{peak}} F_{LD} \, \mathrm{d}l. \tag{3}$$

The example shown in Fig. 2b presents a potential issue for the cleavage experiments. For most cases during the cleavage only the (weak) bonds between the layers are broken, while the layers themselves remain intact in-plane. Taking into account the contribution of friction to the force by removing the baseline, the measured energy is the interlayer cleavage energy. The resulting cleaved stacks can be usually compared to an opened can of sardines (Figure SI 4 and SI 5). In contrast, in the example in Figure 2 the layers were ruptured, which implies a contribution of the intralayer bonds to the total force, leading to an overestimation of the cleavage energy. While this effect is not negligible (see estimation in the SI), only very few experiments show such a rupture and are therefore statistically not relevant for the determination of the cleavage energy. Despite its unrepresentative nature, we show the experiment in Figure 2 because the AFM scans of the usual stacks looking like an "opened can of sardines" are always hampered by the loose layers sticking out.

To benchmark this method, we measure the cleavage energy of graphite, MoS_2 and the weak topological insulator $Bi_{14}Rh_3I_9$. Graphite is chosen, as it is the most investigated, prototype material amongst the layered structures and furthermore its cleavage energy has already been determined by various other techniques. MoS_2 is an important member of the transition metal dichalgogenide family - quasi-2D Van-der-Waals materials with similarly weak inter-layer binding as graphite. Finally, $Bi_{14}Rh_3I_9$ is a layered salt which therefore is expected to represent materials with stronger inter-layer binding due to the ionic contributions.

For graphite in total 21 measurements with five different tips were realized. We found an average value for the cleavage energy of $E_{cl} = 0.35\,\mathrm{J/m^2}$ with a standard deviation of $\sigma(E_{cl}) = \pm 0.06\,\mathrm{J/m^2}$. Our results are in very good agreement with results of $E_{cl} = (0.40 \pm 0.03)\,\mathrm{J/m^2}$ and $E_{cl} = (0.37 \pm 0.02)\,\mathrm{J/m^2}$ from other measurements we consider trustworthy based on the experimental setup.[30,35] Considering all reported values for graphite yields a range from $0.19\,\mathrm{J/m^2}$ to $0.72\,\mathrm{J/m^2}$.[30–33,35,36] This large scatter illustrates the necessity of a reliable and simple method.

We would like to point out the two essential sources for the error that are the calibration of the tip, done once for each tip, and the determination of the surface area. The latter can be mitigated by taking into account only experiments where the cleaved area is well defined in the tapping image after the cleavage process. Concomitantly, these images allow to evaluate whether the experiment involved any in-layer rupture as discussed above. Furthermore, the relative error from determining the area becomes smaller with an increased cleavage area. Therefore, selecting experiments with relatively large cleaved areas yields a smaller error.

Having performed the experiments with five different tips reveals that the error due to the calibration dominates. The standard deviation σ of each set of experiments belonging to the same tip is 0.15, 0.03, 0.06, 0.04, and $0.15\,\mathrm{J/m^2}$, respectively. In contrast, averaging the mean values of the respective sets yields a σ of $0.11\,\mathrm{J/m^2}$, which apart from the first and the last tip, is significantly higher than the σ for each tip. Therefore, a careful calibration and the use of more than one tip for the measurements of the cleavage experiments is advisable.

Finally, provided that the number of experiments is large enough, it is possible to statistically reduce the error bar further by applying an outlier test which considers only the results that are in a range of $\bar{x} \pm 2.5\sigma$. For graphite, this yields in our case nine experiments which lead to a cleavage energy of $(0.36 \pm 0.03)\,\mathrm{J/m^2}$ in contrast to $(0.35 \pm 0.06)\,\mathrm{J/m^2}$ taking into account all 21 experiments.

Table 1 shows a comparison between our experimental data and the lower and upper bounds of theoretical cleavage energies. Both bounds are estimated from a combination of literature data and own calculations. Technical details of the calculations and their relation to available literature data are described in the SI. Our experimental data for graphite fall into the range between the lower theoretical bound, $E_{\mathrm{cl}}^{\mathrm{LB}} = 0.33\ \mathrm{J/m^2}$, and the related upper bound, $E_{\mathrm{cl}}^{\mathrm{UB}} = 0.45\ \mathrm{J/m^2}$.

As an important representative of the dichalcogenide family of layered compounds, we selected MoS_2 for the experimental investigation. This layered material is used on an industrial scale as lubricant,[46] and has been studied in various theoretical papers, see for example

Refs.,[28,47] but experimental data on cleavage or surface energies is scarce.[37,48,49] From the 11 cleavage experiments conducted with two tips and performed according to the procedure described above (Example in the SI: Figure SI 6), we found a mean value of $0.60\,\mathrm{J/m^2}$ with a standard deviation of $\pm 0.19\,\mathrm{J/m^2}$. This value has to be compared to the only experimental data available for MoS_2 which indicates a exfoliation energy of $0.14\,\mathrm{J/m^2}$ (corresponding to a measured surface energy $0.07\,\mathrm{J/m^2}$) derived from a liquid exfoliation study,[48] $0.09\,\mathrm{J/m^2}$ (corresponding to a measured surface energy $0.05\,\mathrm{J/m^2}$) derived from wettability experiments,[49] and a exfoliation energy of $0.22\,\mathrm{J/m^2}$ (corresponding to a measured surface energy of $0.11\,\mathrm{J/m^2}$) from bending MoS_2-layers under the electron microscope.[37] Our measurements provide a significantly larger cleavage energy than the exfoliation energies measured so far with different techniques. However, all these experimental values from the literature are factors of 1.5 to 4 smaller than the theoretical exfoliation energy of $0.33\,\mathrm{J/m^2}$ obtained from the well-established RPA method.[28] They are even smaller than most of the reported experimental values for graphite. This is in strong contrast to our observed success rate of AFM cleavage experiments that is significantly higher for graphite than for MoS_2, suggesting a larger cleavage energy for the latter. Moreover, our experimental value of $0.60\ \mathrm{J/m^2}$ is just below the theoretical upper bound (see Table 1 and SI). We would like mention that in contrast to graphite the observation of an in-layer rupture occurs much more often. Therefore, it is possible that our data suffers a systematic error toward higher cleavage energies. As discussed for graphite, this can be improved systematically by choosing only experiments without in-layer ruptures.

We note that the error bar for our MoS_2 results is notably larger than in the graphite experiment, due to the smaller number of experimental points. Yet, the error bar of our data remains substantially smaller than the dispersion of the results shown in Refs. 48 and 49, whereas the value reported in Ref. 37 was obtained by a single measurement realized on a monolayer of MoS_2. Importantly, the cleavage energy of MoS_2 can be considered as a representative of the transition metal dichalcogenides family including $MoSe_2$, $MoTe_2$,

WSe_2, WS_2 and WTe_2, for which the proposed method could therefore easily be applied (SI: Table SI 5).

Finally, $Bi_{14}Rh_3I_9$ with expected ionic interactions between the layers and therefore stronger inter-layer binding is used to test the limits of the method introduced above. Indeed, the calculated upper bound for the cleavage energy of $Bi_{14}Rh_3I_9$, 0.79 J/m^2, is the largest among all considered compounds. However, this number should not be understood as a strict upper bound for the experimental value since cleavage of $Bi_{14}Rh_3I_9$ was observed to be accompanied by the disruption of atomic layers on a mesoscopic scale.[44] This effect is not considered in the idealized structure model used in our calculation, see details given in the SI. In line with these considerations, the mechanical cleavage by AFM turns out to be more difficult than for the other materials tested and the force curves cannot be used to determine the cleavage energy. This sets an upper limit of the measurable cleavage energy for our method to $E_{cl,max} \approx 0.79\,\mathrm{J/m^2}$. We note that this limit is a very conservative estimate, as we do not know the contribution to the experimental cleavage energy by the mentioned mesoscopic layer-disruptions. Furthermore, this upper limit of $E_{cl,max} \approx 0.79\,\mathrm{J/m^2}$ could be enhanced by using harder AFM cantilevers, with a force constant larger than $45\,\mathrm{N\,m^{-1}}$.

Table 1: Measured cleavage energies, E_{cl}, and related lower and upper theoretical bounds, $E_{\mathrm{cl}}^{\mathrm{LB}}$ and $E_{\mathrm{cl}}^{\mathrm{UB}}$, respectively, in J/m^2. Details of the estimation of the theoretical bounds and results for $MoSe_2$, $MoTe_2$, WS_2, WSe_2, WTe_2 are given in the SI.

	α-C	MoS_2	$Bi_{14}Rh_3I_9$
E_{cl}	0.36 ± 0.03	0.60 ± 0.19	$\gtrsim 0.7$[a]
$E_{\mathrm{cl}}^{\mathrm{LB}}$	0.33	0.35	-
$E_{\mathrm{cl}}^{\mathrm{UB}}$	0.45	0.61	0.79

[a]This energy is an estimation based on the calculated value and experimental observations for MoS_2 and $Bi_{14}Rh_3I_9$

During our investigations we found that, scratching the crystal while exerting a strong force in contact mode successfully introduces a trench into the $Bi_{14}Rh_3I_9$-flake and subsequently allows to remove material (SI: Figure SI 7). While this procedure does not allow to determine cleavage energies, introducing this additional step allows cleavage even of mate-

rials with strong inter-layer interactions and makes the overall AFM-setup an ideal tool to build ultrathin nanodevices. For example, this technique might be very convenient to investigate the influence of the thickness of a single electronic device on its electronic properties by measuring the device properties before and after several cleavage experiments. Moreover, the contacting of ultra thin crystals can become an issue as soon as the thickness reaches a few monolayers. In this context, such a method might offer new ways to study ultra thin crystals with very low ohmic contact resistance by thinning down a rather thick film that has been contacted prior to the cleavage step. We therefore extended an original idea presented in Ref.[41] to a systematic nanostructuring process for layered materials. The example of a WS_2 precontacted ribbon is presented below (Figure 3). In principle, the cleavage energy experiments described above can be used for this purpose. Either one employs the constant height step for the thinning down, as would be sufficient in case of graphite or MoS_2, or one adds the constant force scratching as is necessary for the cleavage of $Bi_{14}Rh_3I_9$. The latter was done for the precontacted WS_2 ribbon, first introducing a scratch in the contact mode (Figure 3b) and subsequently proceeding with the cleavage (Figure 3c).

Summarizing, we developed a technique to measure the cleavage energy of layered materials. This technique is rather simple and does not require any specific set up, apart from an AFM, which is available in most solid state laboratories. It is found to give results in very good agreement with previously reported theoretical and experimental data for graphite and is further used to measure the cleavage energy on a typical Van-der-Waals material (MoS_2) and on a layered salt ($Bi_{14}Rh_3I_9$) with stronger inter-layer binding. The latter measurement was not successful, thus providing an upper limit for the cleavage energy accessible to our method. We complement this experimental work with the theoretical determination of lower and upper bounds for the cleavage energy of the investigated compounds. Finally, we describe how the AFM can be used to thin down Van-der-Waals based electronic devices paving the way to the development of new fabrication processes for low dimensional nanostructures.

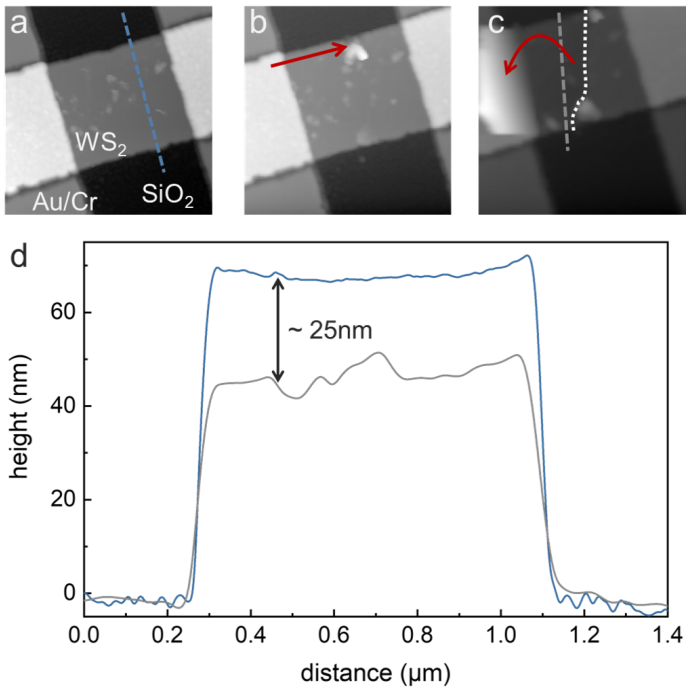

Figure 3: **a**: A WS_2 ribbon contacted with Cr/Au contacts before the cleavage by AFM. **b**: realization of a first scratch on the ribbon (red arrow). **c**: cleavage of the left part of the ribbon (lifted part: red arrow and fissure line: white dotted line). The thickness was reduced by about 25 nm. **d**: height profile before and after cleavage. The two profiles are taken along the two dashed lines in picture **a** and **c** with the corresponding colors.

Acknowledgement

The authors thank Dr. Thomas Mühl and Prof. Dr. Jeroen van den Brink for fruitful discussions and help with the calibration of the cantilever. All authors also thank Ohla Aftenieva, Elkordy Mohamed Shehata and Rohit Acharya for their participation in the project. J.D. acknowledges financial support by the DFG through the SPP 1666 Topological Insulators program (Project No. DU 1376/2-2) and the Würzburg-Dresden Cluster of Excellence on Complexity and Topology in Quantum Matter– ct.qmat (EXC 2147, project-id 0392019). B.R. acknowledges the financial support from the German Research Foundation (DFG) through the Research Fellowship RA 3120/1-1 and from the FCI via a Liebig-Group.

Supporting Information

The supporting information contain the following sections with additional details on the used materials and methods: *Manufacturing the pillars*, *Calibration of the AFM tip*, *Cleavage Experiments* and *Density Functional Calculations*. This material is available free of charge via the internet at http://pubs.acs.org.

TOC graphic

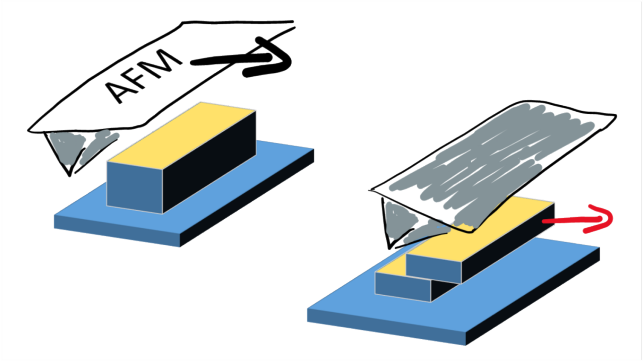

References

(1) Novoselov, K. S.; Geim, A. K.; Morozov, S. V.; Jiang, D.; Zhang, Y.; Dubonos, S. V.; Grigorieva, I. V.; Firsov, A. A. Electric Field Effect in Atomically Thin Carbon Films. *Science* **2004**, *306*, 666–669.

(2) Novoselov, K. S.; Jiang, D.; Schedin, F.; Booth, T. J.; Khotkevich, V. V.; Morozov, S. V.; Geim, A. K. Two-dimensional atomic crystals. *PNAS* **2005**, *102*, 10451–10453.

(3) Hasan, M. Z.; Kane, C. L. Colloquium: Topological insulators. *Review of Modern Physics* **2010**, *82*, 3045–3067.

(4) Qi, X.-L.; Zhang, S.-C. Topological insulators and superconductors. *Review of Modern Physics* **2011**, *83*, 1057–1110.

(5) Schaibley, J. R.; Yu, H.; Clark, G.; Rivera, P.; Ross, J. S.; Seyler, K. L.; Yao, W.; Xu, X. Valleytronics in 2D materials. *Nature Reviews Materials* **2016**, *1*, 16055.

(6) Qian, X.; Liu, J.; Fu, L.; Li, J. Quantum spin Hall effect in two-dimensional transition metal dichalcogenides. *Science* **2014**, *346*, 1344.

(7) Sajadi, E.; Palomaki, T.; Fei, Z.; Zhao, W.; Bement, P.; Olsen, C.; Luescher, S.; Xu, X.; Folk, J. A.; Cobden, D. H. Gate-induced superconductivity in a monolayer topological insulator. *Science* **2018**, *362*, 922–925.

(8) Fatemi, V.; Wu, S.; Cao, Y.; Bretheau, L.; Gibson, Q. D.; Watanabe, K.; Taniguchi, T.; Cava, R. J.; Jarillo-Herrero, P. Electrically tunable low-density superconductivity in a monolayer topological insulator. *Science* **2018**, *362*, 926–929.

(9) Ma, Q. et al. Observation of the nonlinear Hall effect under time-reversal-symmetric conditions. *Nature* **2019**, *565*, 337–342.

(10) Wu, S.; Fatemi, V.; Gibson, Q. D.; Watanabe, K.; Taniguchi, T.; Cava, R. J.; Jarillo-Herrero, P. Observation of the quantum spin Hall effect up to 100 kelvin in a monolayer crystal. *Science* **2018**, *359*, 76.

(11) Kang, K.; Li, T.; Sohn, E.; Shan, J.; Mak, K. F. Nonlinear anomalous Hall effect in few-layer WTe2. *Nature Materials* **2019**, *18*, 324–328.

(12) Gong, C.; Li, L.; Li, Z.; Ji, H.; Stern, A.; Xia, Y.; Cao, T.; Bao, W.; Wang, C.; Wang, Y.; Qiu, Z. Q.; Cava, R. J.; Louie, S. G.; Xia, J.; Zhang, X. Discovery of intrinsic ferromagnetism in two-dimensional van der Waals crystals. *Nature (London)* **2017**, *546*, 265.

(13) Cao, Y.; Fatemi, V.; Fang, S.; Watanabe, K.; Taniguchi, T.; Kaxiras, E.; Jarillo-Herrero, P. Unconventional superconductivity in magic-angle graphene superlattices. *Nature* **2018**, *556*, 43.

(14) Cao, Y.; Fatemi, V.; Demir, A.; Fang, S.; Tomarken, S. L.; Luo, J. Y.; Sanchez-Yamagishi, J. D.; Watanabe, K.; Taniguchi, T.; Kaxiras, E.; Ashoori, R. C.; Jarillo-Herrero, P. Correlated insulator behaviour at half-filling in magic-angle graphene superlattices. *Nature* **2018**, *556*, 80.

(15) Asaba, T.; Wang, Y.; Li, G.; Xiang, Z.; Tinsman, C.; Chen, L.; Zhou, S.; Zhao, S.; Laleyan, D.; Li, Y.; Mi, Z.; Li, L. Magnetic Field Enhanced Superconductivity in Epitaxial Thin Film WTe2. *Scientific Reports* **2018**, *8*, 6520.

(16) Girifalco, L. A.; Lad, R. A. Energy of Cohesion, Compressibility, and the Potential Energy Functions of the Graphite System. *J. Chem. Phys.* **1956**, *25*, 693–697.

(17) Charlier, J.-C.; Gonze, X.; Michenaud, J.-P. Graphite Interplanar Bonding: Electronic Delocalization and van der Waals Interaction. *EPL* **1994**, *28*, 403–408.

(18) Wang, Y.; Scheerschmidt, K.; Gösele, U. Theoretical investigations of bond properties in graphite and graphitic silicon. *Phys. Rev. B* **2000**, *61*, 12864–12870.

(19) Rydberg, H.; Dion, M.; Jacobson, N.; Schröder, E.; Hyldgaard, P.; Simak, S. I.; Langreth, D. C.; Lundqvist, B. I. Van der Waals Density Functional for Layered Structures. *Phys. Rev. Lett.* **2003**, *91*, 126402.

(20) Rydberg, H.; Jacobson, N.; Hyldgaard, P.; Simak, S. I.; Lundqvist, B. I.; Langreth, D. C. Hard numbers on soft matter. *Surface Science* **2003**, *532-535*, 606–610.

(21) Hasegawa, M.; Nishidate, K. Semiempirical approach to the energetics of interlayer binding in graphite. *Phys. Rev. B* **2004**, *70*, 205431.

(22) Ortmann, F.; Bechstedt, F.; Schmidt, W. G. Semiempirical van der Waals correction to the density functional description of solids and molecular structures. *Phys. Rev. B* **2006**, *73*, 205101.

(23) Hasegawa, M.; Nishidate, K.; Iyetomi, H. Energetics of interlayer binding in graphite: The semiempirical approach revisited. *Phys. Rev. B* **2007**, *76*, 115424.

(24) Ziambaras, E.; Kleis, J.; Schröder, E.; Hyldgaard, P. Potassium intercalation in graphite: A van der Waals density-functional study. *Phys. Rev. B* **2007**, *76*, 155425.

(25) Savini, G.; Dappe, Y. J.; Öberg, S.; Charlier, J. C.; Katsnelson, M. I.; Fasolino, A. Bending modes, elastic constants and mechanical stability of graphitic systems. *Carbon* **2011**, *49*, 62–69.

(26) Spanu, L.; Sorella, S.; Galli, G. Nature and Strength of Interlayer Binding in Graphite. *Phys. Rev. Lett.* **2009**, *103*, 196401.

(27) Lebègue, S.; Harl, J.; Gould, T.; Ángyán, J. G.; Kresse, G.; Dobson, J. F. Cohesive Properties and Asymptotics of the Dispersion Interaction in Graphite by the Random Phase Approximation. *Phys. Rev. Lett.* **2010**, *105*, 196401.

(28) Björkman, T.; Gulans, A.; Krasheninnikov, A. V.; Nieminen, R. M. van der Waals Bonding in Layered Compounds from Advanced Density-Functional First-Principles Calculations. *Phys. Rev. Lett.* **2012**, *108*, 235502.

(29) Benedict, L. X.; Chopra, N. G.; Cohen, M. L.; Zettl, A.; Louie, S. G.; Crespi, V. H. Microscopic determination of the interlayer binding energy in graphite. *Chemical Physics Letters* **1998**, *286*, 490–496.

(30) Zacharia, R.; Ulbricht, H.; Hertel, T. Interlayer cohesive energy of graphite from thermal desorption of polyaromatic hydrocarbons. *Phys. Rev. B* **2004**, *69*, 155406.

(31) Kis, A.; Jensen, K.; Aloni, S.; Mickelson, W.; Zettl, A. Interlayer Forces and Ultralow Sliding Friction in Multiwalled Carbon Nanotubes. *Phys. Rev. Lett.* **2006**, *97*, 025501.

(32) Liu, Z.; Liu, J. Z.; Cheng, Y.; Li, Z.; Wang, L.; Zheng, Q. Interlayer binding energy of graphite: A mesoscopic determination from deformation. *Phys. Rev. B* **2012**, *85*, 205418.

(33) Roenbeck, M. R.; Wei, X.; Beese, A. M.; Naraghi, M.; Furmanchuk, A.; Paci, J. T.; Schatz, G. C.; Espinosa, H. D. In Situ Scanning Electron Microscope Peeling To Quantify Surface Energy between Multiwalled Carbon Nanotubes and Graphene. *ACS Nano* **2014**, *8*, 124–138.

(34) Koren, E.; Lörtscher, E.; Rawlings, C.; W., K. A.; Duerig, U. Adhesion and friction in mesoscopic graphite contacts. *Science* **2015**, *348*, 679–683.

(35) Wang, W.; Dai, S.; Li, X.; Yang, J.; Srolovitz, D. J.; Zheng, Q. Measurement of the cleavage energy of graphite. *Nat. Commun.* **2015**, *6*, 7853.

(36) van Engers, C. D.; Cousens, N. E. A.; Babenko, V.; Britton, J.; Zappone, B.; Grobert, N.; Perkin, S. Direct Measurement of the Surface Energy of Graphene. *Nano Lett.* **2017**, *17*, 3815–3821.

(37) Tang, D.-M.; Kvashnin, D. G.; Najmaei, S.; Bando, Y.; Kimoto, K.; Koskinen, P.; Ajayan, P. M.; Yakobson, B. I.; Sorokin, P. B.; Lou, J.; Golberg, D. Nanomechanical cleavage of molybdenum disulphide atomic layers. *Nat. Commun.* **2014**, *5*, 3631.

(38) Tseng, A. A.; Notargiacomo, A.; Chen, T. P. Nanofabrication by scanning probe microscope lithography: A review. *J. Vac. Sci. & Tech. B: Microelec. Nano. Struc. Proc., Measure., Phenom.* **2005**, *23*, 877–894.

(39) Malekian, M.; Park, S. S.; Strathearn, D.; Mostofa, M. G.; Jun, M. B. G. Atomic force microscope probe-based nanometric scribing. *J. Micromech. Microeng.* **2010**, *20*, 115016.

(40) Tseng, A. A. Removing Material Using Atomic Force Microscopy with Single- and Multiple-Tip Sources. *Small* **2011**, *7*, 3409–3427.

(41) Hong, S. S.; Kundhikanjana, W.; Cha, J. J.; Lai, K.; Kong, D.; Meister, S.; Kelly, M. A.; Shen, Z.-X.; Cui, Y. Ultrathin Topological Insulator Bi2Se3 Nanoribbons Exfoliated by Atomic Force Microscopy. *Nano Lett.* **2010**, *10*, 3118–3122.

(42) Rasche, B.; Isaeva, A.; Ruck, M.; Borisenko, S.; Zabolotnyy, V.; Büchner, B.; Koepernik, K.; Ortix, C.; Richter, M.; van den Brink, J. Stacked topological insulator built from bismuth-based graphene sheet analogues. *Nat. Mater.* **2013**, *12*, 422–425.

(43) Rasche, B.; Isaeva, A.; Gerisch, A.; Kaiser, M.; Van den Broek, W.; Koch, C. T.; Kaiser, U.; Ruck, M. Crystal Growth and Real Structure Effects of the First Weak 3D Stacked Topological Insulator $Bi_{14}Rh_3I_9$. *Chemistry of Materials* **2013**, *25*, 2359–2364.

(44) Pauly, C.; Rasche, B.; Koepernik, K.; Liebmann, M.; Pratzer, M.; Richter, M.; Kellner, J.; Eschbach, M.; Kaufmann, B.; Plucinski, L.; Schneider, C. M.; Ruck, M.; van den Brink, J.; Morgenstern, M. Subnanometre-wide electron channels protected by topology. *Nat. Phys.* **2015**, *11*, 338–343.

(45) Varenberg, M.; Etsion, I.; Halperin, G. An improved wedge calibration method for lateral force in atomic force microscopy. *Rev. Sci. Instrum.* **2003**, *74*, 3362.

(46) Vazirisereshk, M. R.; Martini, A.; Strubbe, D. A.; Baykara, M. Z. Solid Lubrication with MoS2: A Review. *Lubr.* **2019**, *7*, 57.

(47) Nikiforov, I.; Tang, D.-M.; Wei, X.; Dumitrică, T.; Golberg, D. Nanoscale Bending of Multilayered Boron Nitride and Graphene Ribbons: Experiment and Objective Molecular Dynamics Calculations. *Phys. Rev. Lett.* **2012**, *109*, 025504.

(48) Coleman, J. N. et al. Two-Dimensional Nanosheets Produced by Liquid Exfoliation of Layered Materials. *Science* **2011**, *331*, 568–571.

(49) Gaur, A. P. S.; Sahoo, S.; Ahmadi, M.; Dash, S. P.; Guinel, M. J.-F.; Katiyar, R. S. Surface Energy Engineering for Tunable Wettability through Controlled Synthesis of MoS2. *Nano Letters* **2014**, *14*, 4314–4321.